Journal of The Electrochemical Society, **157** (5) A617-A624 (2010)
0013-4651/2010/157(5)/A617/8/$28.00 © The Electrochemical Society

High Performance $LiCoO_2$ Cathode Materials at 60°C for Lithium Secondary Batteries Prepared by the Facile Nanoscale Dry-Coating Method

Yonghyun Cho, Junho Eom, and Jaephil Cho[*,z]

School of Energy Engineering, Ulsan National Institute of Science and Technology, Ulsan 689-798, Korea

A mass scalable dry-coating method was used on a $LiCoO_2$ cathode to improve cycling stability at 60°C and, in contrast to the conventional wet-coating method, this one did not require a solvent. Electrochemical results of the MgF_2, Al_2O_3, and TiO_2 coatings on $LiCoO_2$ cathodes showed a fast capacity fade, resulting in <10% capacity retention at 60°C under 1C rate cycling, whereas an uncoated cathode showed 64% retention. This difference was believed to be because the residual coating layers which did not react with the bulk layer accelerated the side reactions with the electrolytes at 60°C, leading to increased formation of the surface films. However, when $MgCO_3$ and $AlPO_4$ were used for dry coating, the coating layers completely disappeared, but a higher concentration of coating elements was found near the surfaces. Overall, the cathodes coated with $MgCO_3$ and $AlPO_4$ exhibited 79 and 88% capacity retention, respectively, at 60°C under 1C rate cycling.
 [DOI: 10.1149/1.3332676]

Manuscript submitted December 22, 2009; revised manuscript received January 22, 2010. Published April 9, 2010.

Recent application of the Li-ion cells has been extended to energy storage devices for solar cells, wind, and hybrid electrical vehicles.[1,2] Thus, battery performances both at room temperature and at ambient temperatures (e.g., 60°C) become more important issues, along with volumetric energy density. Among the cathode materials, the most spotlighted candidates are $LiCoO_2$ and $LiNi_{1-x-y}Co_xM_yO_2$.[3-15] Between them, $LiCoO_2$ has the highest electrode density with 3.7 g/cm^3, whereas the latter has only 3.3 g/cm^3.[3] Increasing the cutoff voltage is an alternative way to increase the volumetric energy density of the cell, but it leads to structural instability of the cathodes at elevated temperatures (>50°C).

This instability accelerates the dissolution of the electrochemically active metal ions, in turn, accelerating the destruction of the lithium insertion/extraction sites at the surface.[4,5] Moreover, large internal strains and subsequent mechanical degradation of the cathode materials enhance the structural degradation of the cathodes.[16] In addition, dissolved Li^+ ions are solvated and combine with oxidized solvent molecules to form lithium-containing organic products. This effect becomes evident during storage and cycling at elevated temperatures above 60°C.[3] Due to concurrently occurring side reactions with the electrolytes at the particle surface and continuous structural destruction from the dissolution of Li and Co ions from the cathode, the capacity of $LiCoO_2$ rapidly fades. Therefore it is important to form a protective coating layer near the surfaces to sustain lithium diffusion and to keep a reasonable electronic conductivity. Many studies have focused on the development of a coated $LiCoO_2$ by the wet-coating process,[5,17-20] and so far, the wet-coating method is the popular method even though it uses a solvent and an additional drying process is required. At this point, direct coating with a coating material on the cathode powder is the best method, but, as expected, electrochemical properties may vary with the coating material. $AlPO_4$ and MgO coatings prepared by a sol–gel method (wet-coating method) have been reported,[10,13] but these coatings on the cathodes using a direct coating method have not been explored.

In this study, we investigate the structural changes and interfacial behavior of $LiCoO_2$ coated with various metal oxides by the dry-coating method by using an electrochemical cycling test at 60°C. Cycling stability at 60°C has been ignored in $LiCoO_2$ and $LiNi_{1-x-y}Co_xM_yO_2$ cathodes despite their performing importance at this temperature. By testing coating candidates at 60°C, optimized dry-coating materials can be selected. Among them, $AlPO_4$- and $MgCO_3$-coated $LiCoO_2$ cathodes demonstrated much improved cycling results than uncoated and Al_2O_3-, TiO_2-, and MgF_2-coated ones.

Experimental

A nanosized coating material was used for the dry coating. This is important as the material must be uniformly mixed with the bulk $LiCoO_2$ (L&F New Materials, Korea). As-received coating materials were ballmilled using a high impact milling machine to get a particle size of ~100 nm. In this experiment, 100 nm metal oxide nanoparticles were physically mixed with 20 μm sized $LiCoO_2$ cathodes in a mechanical mixer with a rotating speed of 150 rpm for 20 h. This coating concentration was varied between 0.2 and 1 wt % coating concentrations (the weight of the cathode was fixed at 3 kg). For instance, a 1 wt % coating concentration refers to 30 g of metal oxide per 3 kg of $LiCoO_2$ powder. The resulting mixed powder was fired at 1000°C for 5 h in air and then slowly cooled to room temperature. Based upon thermal gravimetric analysis of the uncoated sample, no weight loss occurred at 1000°C for 5 h. The stoichiometry of lithium in the uncoated Li_xCoO_2 powder was 1.01 and, after coating, it exhibited a stoichiometry of 1 based upon inductively coupled plasma–mass spectroscopy.

The wet-coating method was referred from Ref. 5. A coin-type half-cell (2016-size) contained a test electrode, a lithium-metal counter-and-reference electrode, a 15 μm thick microporous polyethylene separator, and an electrolyte solution of 1.05 M $LiPF_6$ in ethylene carbonate/dimethyl carbonate (1:1 vol %) (LG Chem., Korea). Normally, the amount of active materials in the cathode composite was 19 mg. The cathodes for the battery test cells were made from the cathode material, Super P carbon black, and poly(vinylidene fluoride) binder (Solef) in a weight ratio of 94:3:3. The electrodes were prepared by coating a cathode slurry onto Al foil followed by drying at 130°C for 20 min and, finally, by roll-pressing. For cycling tests, five cells were used, and the standard deviation of the cells was ±2 mAh/g.

Electrochemical impedance spectroscopy (EIS) data were collected before and after 30 cycles at 60°C with an ac amplitude of 10 mV in the frequency range of 0.5 MHz–10 mHz by an Ivium impedance analyzer. The EIS measurements of the cell before and after cycling were done after cell assemblage and after discharging to 3 V, respectively. All the fittings were carried out with a Solartron software "Zview" having a "fit circle" function after discharging to 3 V. The resistance values and time constant (T_{ct}) were deduced from this software. Powder X-ray diffractometer (XRD, D/Max2000, Rigaku) measurements using Cu Kα radiation was used to identify the phase, and the JCPDS card no. of $LiCoO_2$ (PDF no. 50-0653), Co_3O_4 (no. 42-1467), and TiO_2 (anatase, no. 78-2468) were used for phase identification. The surface of the uncoated and coated samples

* Electrochemical Society Active Member.
z E-mail: jpcho@unist.ac.kr

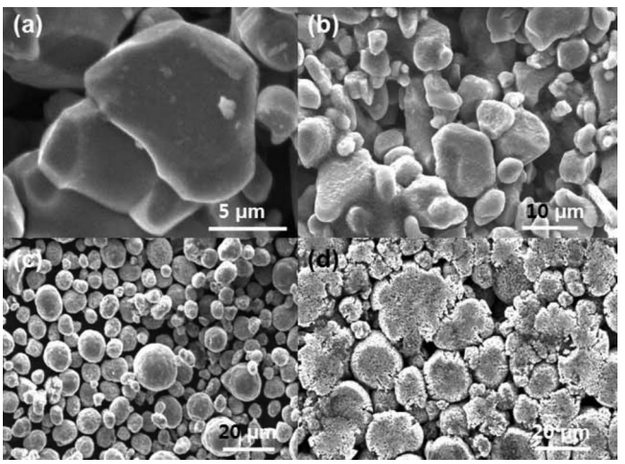

Figure 1. SEM images of the (a) $LiCoO_2$ and (b) $LiNi_{0.8}Co_{0.15}Al_{0.05}O_2$ cathode electrodes [(a) and (c)] before and [(b) and (d)] after pressing.

was observed using a scanning electron microscope (SEM, JSM 6400, JEOL) and a transmission electron microscope (TEM, JEOL 2010F). TEM samples were prepared by evaporation of the dispersed nanoparticles in acetone or hexane on carbon-coated copper grids.

Results and Discussion

First, we need to compare the morphological changes of $LiCoO_2$ to a $LiNi_{0.8}Co_{0.15}Al_{0.05}O_2$ cathode electrode after pressing. Figure 1 shows the SEM images of the (a) $LiCoO_2$ and (c) $LiNi_{0.8}Co_{0.15}Al_{0.05}O_2$ cathode electrodes [(a) and (c)] before and [(b) and (d)] after roll-pressing. (After evaporating the *n*-methyl pyrrolidone solvent in the electrode in an oven, it should be pressed to increase the adhesion with the current collector.) The $LiNi_{0.8}Co_{0.15}Al_{0.05}O_2$ cathode consists of aggregated nanosized primary particles. After pressing, they cannot maintain their pristine morphology and are pulverized to small-sized ones. $LiCoO_2$ particles show no morphological changes even after pressing. Such pulverized Ni-based cathode materials with an increased surface area have more chances to expose the reactions with the electrolytes, which mean a much degraded elevated temperature performance, especially cycling performance above 60°C. In this regard, $LiCoO_2$ is expected to show a much enhanced structural stability at elevated storage performance.[18]

Figure 2 shows the SEM images of the uncoated and Al_2O_3-coated $LiCoO_2$ particles, but it does not show any difference in surface morphology between the two due to the formation of the nanoscale coating layer. The energy-dispersive X-ray (EDX) profile of Al_2O_3-coated $LiCoO_2$ particles (Fig. 3) exhibits the uniformly distributed Al elements throughout the particles. Figure 4 shows the XRD patterns of the uncoated and coated $LiCoO_2$ with various coating materials via the dry-coating method, for which Miller indexes

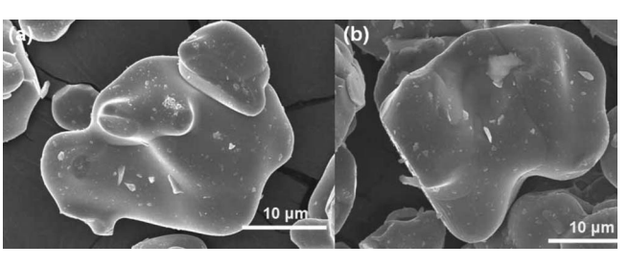

Figure 2. SEM images of (a) the uncoated and (b) Al_2O_3-coated $LiCoO_2$ particles.

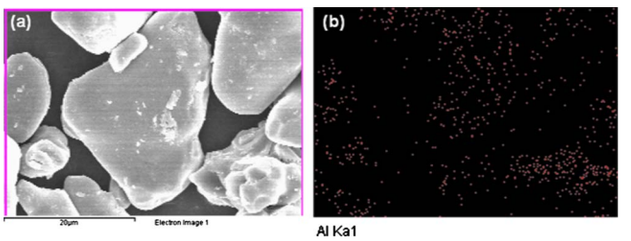

Figure 3. (Color online) SEM images of (a) Al_2O_3-coated $LiCoO_2$ particles and (b) EDX profile of Al elements in (a).

(*hkl*) are indexed for a hexagonal setting. They do not show any secondary phases. The lattice constants *a* and *c* did not show any variation relative to the coated TiO_2 and Al_2O_3-coated samples. For instance, the *a* and *c* values (2.816 and 14.035 Å, respectively) of the uncoated sample remained almost constant even after TiO_2 coating (see Table I). The larger intensity of the (006) peak than that of the (102) peak is indicative of an increased distortion along the *c*-axis. This result is consistent with *c*/*a* ratios in Table I. SEM and XRD results may indicate that the dry-coating method is expected to lead to the formation of a solid solution phase with a higher concentration of coating metal elements confined near the surfaces. If the residual coating layer is present, its layer may be irregular with a different coating thickness.

Figure 5 shows high resolution electron microscope (HREM) images of uncoated and coated cathodes with Al_2O_3, TiO_2, and MgF_2. Because all coating metal oxides with an average particle size of <100 nm were annealed at 1000°C for 5 h, the coating materials were expected to completely react with $LiCoO_2$. However, as can be seen in the images, MgF_2 and Al_2O_3-coated cathodes show an amorphous coating layer of <4 nm. TiO_2 shows the clear presence of a crystalline coating layer consisting of an anatase phase with an ir-

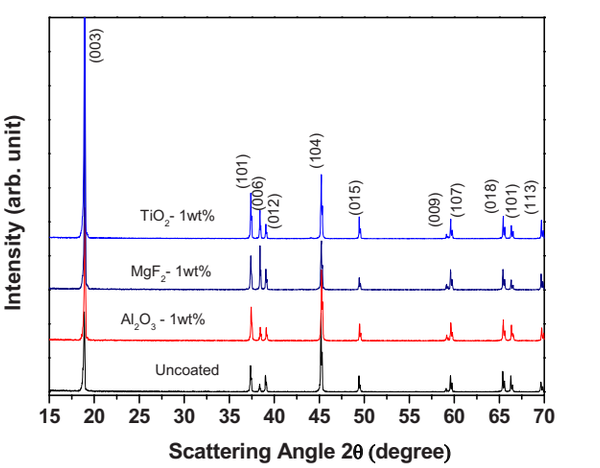

Figure 4. (Color online) XRD patterns of the uncoated and TiO_2-, MgF_2-, and Al_2O_3-coated $LiCoO_2$ cathode materials via the dry-coating method.

Table I. XRD lattice constants *a* and *c* of uncoated and coated $LiCoO_2$ with TiO_2, MgF_2, and Al_2O_3.

Material	*a* (±0.002 Å)	*c* (±0.002 Å)	*c*/*a*
Uncoated $LiCoO_2$	2.816	14.034	4.983
TiO_2	2.815	14.035	4.985
MgF_2	2.815	14.036	4.986
Al_2O_3	2.815	14.036	4.986

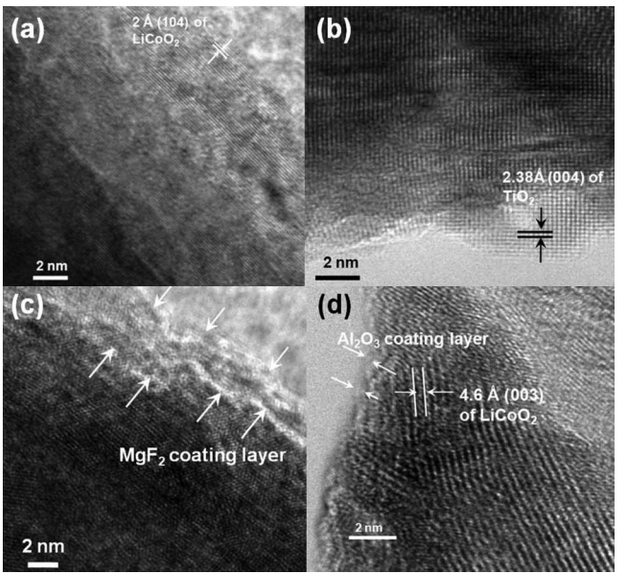

Figure 5. TEM images of the (a) uncoated and (b) TiO_2-, (c) MgF_2-, and (d) Al_2O_3-coated $LiCoO_2$ via the dry-coating method.

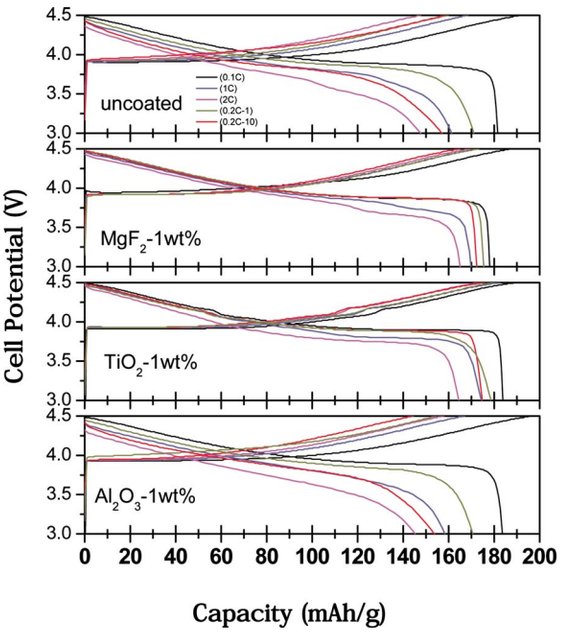

Figure 7. (Color online) Voltage profiles of uncoated and coated $LiCoO_2$ with MgF_2, Al_2O_3, and TiO_2 under various C rates between 3 and 4.5 V in coin-type half-cells at 21°C. After each cycle at 0.1, 1, and 2C rates, the cells were cycled for 10 cycles at 0.2C rate.

regular coating thickness (<2 nm). Because of the annealing temperature, it was also highly plausible that a solid solution phase was also formed at the interfacial regions as a result of the reaction between $LiCoO_2$ and the coating material.

Using these coated cathodes, we investigate the rate capability and cyclability of the uncoated and coated $LiCoO_2$ with MgF_2, Al_2O_3, and TiO_2 under various C rates between 3 and 4.5 V in coin-type half-cells at 21°C (Fig. 6a) (for voltage profiles, see Fig. 7). Although the rate capability of the uncoated sample at the 2C rate is vastly inferior to the other coated cathodes, the first discharge capacity is comparative to the others, showing 182 mAh/g at 0.1C rate. At 2C rate, the MgF_2-coated cathode has the highest capacity retention of 93%, followed by the TiO_2-coated and uncoated cathodes, showing 89 and 81%, respectively. However, the retention values of the Al_2O_3-coated cathode are similar to those of the uncoated cathode. The TiO_2-coated sample exhibits the highest capacity after 10 cycles at a rate of 0.2C, showing 183 mAh/g.

Figure 6b shows cycling test results at 60°C, and after finishing the rate capability to 2C, the cells were cycled at a rate of 0.2C up to 10 cycles (test condition was identical to 21°C). However, similar to room temperature, the TiO_2- and MgF_2-coated cathodes show the highest discharge capacities and rate capability (see Fig. 8). The rate capability of the MgF_2- and TiO_2-coated cathodes are 91 and 94%, respectively, at 2C rate. However, the discharge capacity of the TiO_2-coated cathode after 10 cycles is the highest value among the samples, showing 183 mAh/g. Conversely, at 60°C, the rate capability of the Al_2O_3-coated cathode is improved by 7% compared to that at 21°C. The rate capability of the cathode also relies on its electronic conductivity affected by the temperature and its surface nature. For instance, increasing the cell testing temperature and electronic coating materials can enhance the rate capability. The larger capacity fade of the coated samples at 21°C than at 60°C upon increasing the rate from 0.2 to 2C may be related to the nature of the coating layer. Unreacted nonconducting Al_2O_3, TiO_2, and TiO_2 coating layers prepared by a dry-coating method may impede the electronic conductivity at 21°C.

However, surprisingly, when cycling at 1C rate out to 30 cycles at 60°C, quite a different phenomenon is observed. Figure 9 shows the cycling results of the MgF_2-, Al_2O_3-, and TiO_2-coated $LiCoO_2$, prepared by dry coating at 60°C, and after increasing the rate to 1C, it continues to cycle up to 30 cycles (see Fig. 10). Except for the uncoated sample, the other cells containing coated cathodes show severe capacity fade and a large polarization at 1C rate cycling. After 30 cycles, the discharge capacities of all the cells were below 20 mAh/g, and all the coated cathodes show significant polarization except for the TiO_2-coated cathode prepared by the wet-coating method. Surprisingly, the TiO_2-coated sample prepared by the wet-coating method maintains 141 mAh/g after 30 cycles.

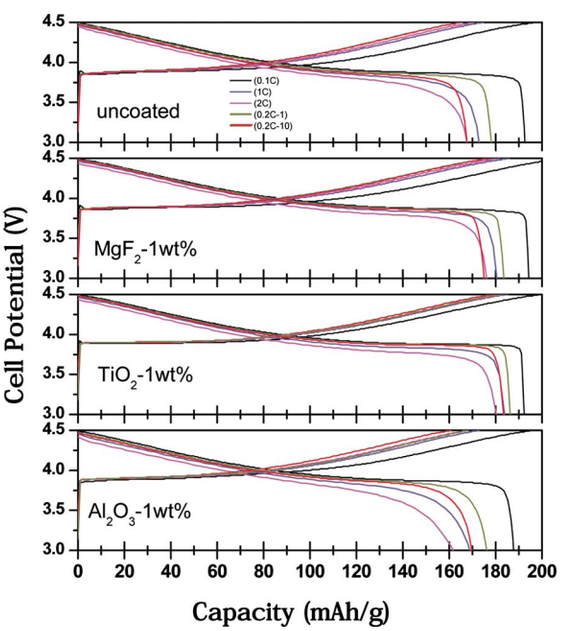

Figure 8. (Color online) Voltage profiles of uncoated and coated $LiCoO_2$ with MgF_2, Al_2O_3, and TiO_2 under various C rates between 3 and 4.5 V in coin-type half-cells at 60°C. After each cycle at 0.1, 1, and 2C rates, the cells were cycled for 10 cycles at 0.2C rate.

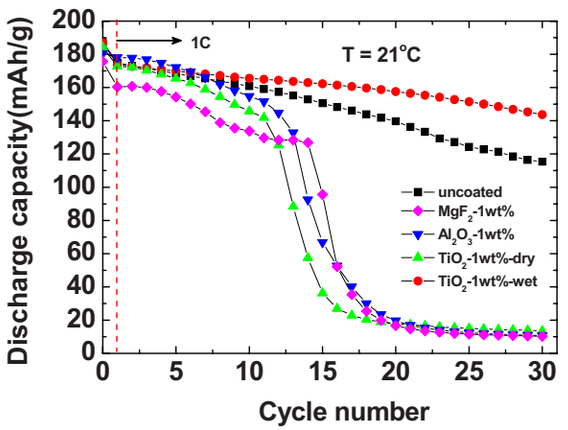

Figure 9. (Color online) Plots of discharge capacity of uncoated and MgF_2-, Al_2O_3-, and TiO_2 (wet and dry coatings)-coated cathodes under various C rates at 60°C. (After each cycle at a rate of 0.1C, cells were cycled at a rate of 1C for 30 cycles.)

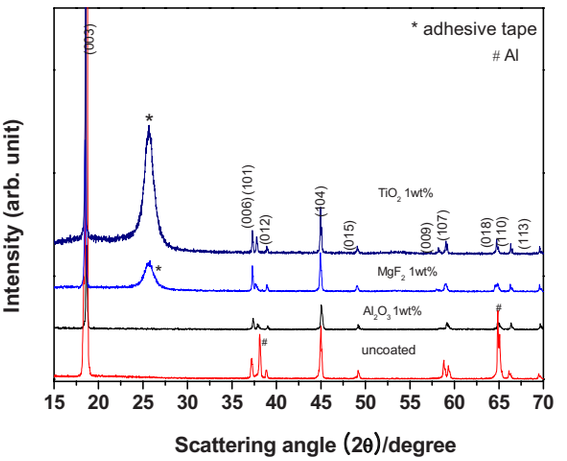

Figure 11. (Color online) XRD pattern analysis of the uncoated and coated $LiCoO_2$ with 1 wt % MgF_2, Al_2O_3, and TiO_2 nanoparticles after cycling at a rate of 1C for 30 cycles at 60°C.

This result may show problems with the dry-coating method. In the uncoated $LiCoO_2$, it demonstrated severe structural degradation during storage at 80°C and CoO and Co_3O_4 formation by means of Co^{4+} reduction.[5] However, even after coating, such a rapid capacity fade may indicate severe structural degradation or substantially increased thickness of the surface films at the cathode. To elucidate such an origin, an XRD pattern analysis of the cycled electrode was carried out, but it did not show any formation of secondary phases (Fig. 11). The lattice constants of the uncoated cathodes show a slight contraction after 30 cycles, and the peak broadening factor (Δk) (full width at half-maximum) is 0.04, which is 5 times higher than before the cycle (see Table II). Other coated materials did not show such peak broadening ($\Delta k = 0.005$), which was quite identical to those cycled at room temperature. An increased Δk value may indicate the formation of microstructural defects in the cathode[19] and, therefore, the capacity fade of these coated samples is not related to such defects.

A more detailed analysis was carried out using the HREM, as shown in Fig. 12. An uncoated sample obtained after 60°C cycles shows the partial presence of lattice fringes corresponding to the (311) planes of the Co_3O_4 phase. Large internal strains and subsequent mechanical degradation of the cathode materials originate from the dissolution of Li^+ ions and reduction of highly oxidized Co^{4+} ions, and the formation of by-products between the reaction-dissolved ions and electrolytes at the interface enhances the structural degradation of the cathodes.[20] This effect was evident during storage at elevated temperatures. It is believed that such Co^{4+}-ion reduction initiates structural rearrangement from the layered phase to the spinel phase. In general, the transformation of the layered structure with the $R\bar{3}m$ space group to the spinel phase ($Fd\bar{3}m$)

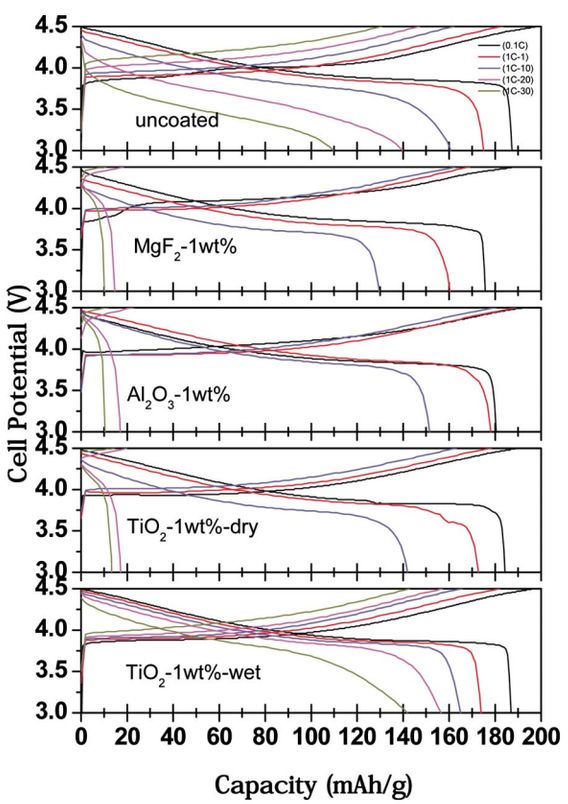

Figure 10. (Color online) Voltage profiles of uncoated and coated $LiCoO_2$ with MgF_2, Al_2O_3, and TiO_2 under various C rates between 3 and 4.5 V in coin-type half-cells at 60°C. At 1C rate, cells continued to cycle up to 30 cycles.

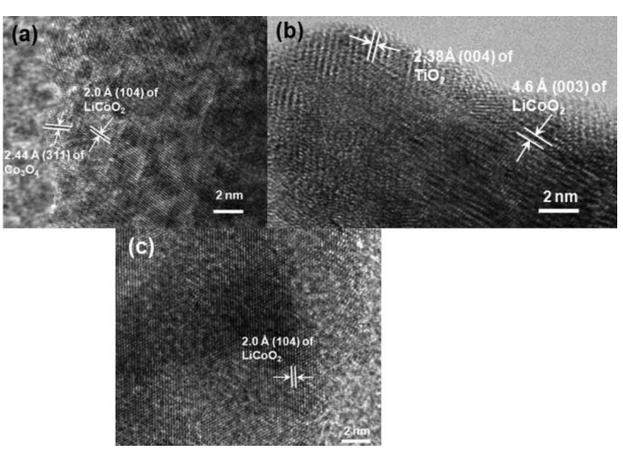

Figure 12. HREM images of (a) the uncoated and [(b) and (c)] 1 wt % TiO_2- and Al_2O_3-coated $LiCoO_2$ via dry-coating method after 30 cycles at a rate of 1C at 60°C.

Table II. XRD lattice constants *a* and *c* and peak broadening factor (Δk) of uncoated and coated $LiCoO_2$ with TiO_2, MgF_2, and Al_2O_3 after 30 cycles at a rate of 1C under 60°C.

Material	*a* (±0.002 Å)	*c* (±0.002 Å)	(Δk) (±0.003)
Uncoated $LiCoO_2$	2.814	14.032	0.04
TiO_2	2.815	14.035	0.005
MgF_2	2.816	14.034	0.004
Al_2O_3	2.815	14.034	0.005

requires the migration of 25% of the transition-metal ions from 3b octahedral sites (metal layer) to 3a octahedral sites (lithium layer). A similar result to this was observed in the uncoated Li_xCoO_2 cathode charged at 4.5 V at the particle surface after storage at 90°C for 4 h.[5]

However, the TEM images of the TiO_2- and Al_2O_3-coated samples (Fig. 12b and c) do not show any secondary phases on the particle surfaces and only show $LiCoO_2$ lattice fringes, which is consistent with their XRD patterns. (In the Al_2O_3-coated sample, after cycling, the amorphous coating layer was difficult to observe due to the binder and carbon black.) However, the TiO_2-coated cathode prepared by wet coating showed a crystalline coating layer on the surface. The wet-coating method was used on Ti isopropoxide for a precursor and isopropyl alcohol solvent. Hence, during firing, all the Ti elements in the precursor were fully incorporated with the $LiCoO_2$, thus possibly forming a $LiCo_{1-x}Ti_xO_2$ solid solution. The formation of the solid solution phase has been proposed in various wet-coating methods.[4,5,9] Conversely, the TiO_2-coated cathode prepared by a dry-coating method shows a TiO_2 coating layer on the surface. Although we expect that the TiO_2 nanoparticle could react with $LiCoO_2$ at 1000°C, it may not form a complete solid solution, and the remaining TiO_2 resides on the particle surface, which may cause the eventual increasing formation of nonconducting surface films at the interface, leading to a rapid capacity fade.

To investigate the difference in capacity fading between the coated cathodes, EIS analysis after 30 cycles at 60°C was carried out. Figure 13 shows Nyquist plots of coin-type half-cells containing uncoated and coated cathodes before and after cycling at 60°C and the interfacial behavior between them; the electrolyte can be investigated by using a possible equivalent circuit as proposed. The values of R_{SEI} (surface film resistance), R_{ct} (charge-transfer resistance), and T_{ct} can be estimated from the Nyquist plot and are summarized in Table III. Before cycling, R_{ct} values of the cathodes are quite small regardless of coating, which could be related to the fact that coating does not affect the electronic conductivity of the cathode. The EIS spectra of the uncoated, wet TiO_2 and dry TiO_2 cathodes after cycling show small tails at the end of the circles (low frequency), which indicates the initiation of the Warburg impedances. A similar behavior is also observed in charging or cycled electrodes.[21,22]

After cycling, the values of R_{SEI} and R_{ct} in the coated samples are quite similar to each other except for the TiO_2-coated sample

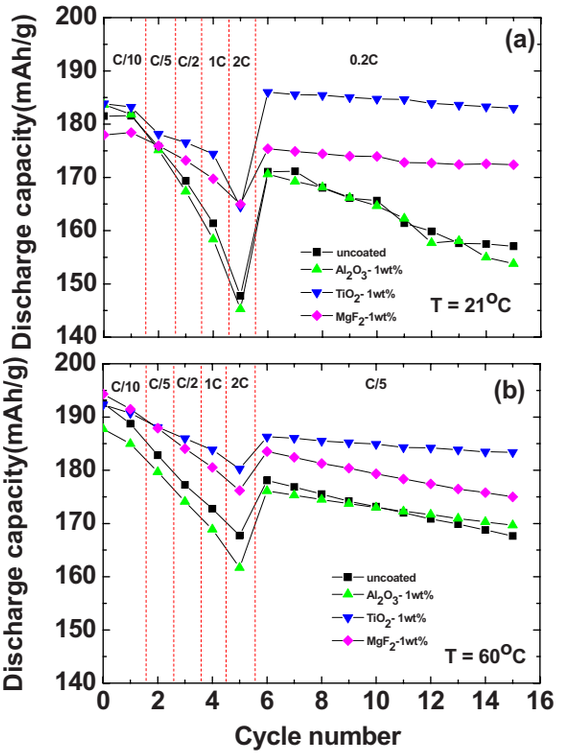

Figure 6. (Color online) Plots of discharge capacity of uncoated and MgF_2-, Al_2O_3-, and TiO_2-coated cathodes under various C rates at 21 and 60°C (cells were finally cycled at a rate of 0.2C for 10 cycles).

prepared by the dry-coating method and the uncoated one. R_{ct} of the Al_2O_3- and MgF_2-coated cathodes are almost a 49-fold increase compared to the TiO_2-coated one obtained from the wet-coating method. Moreover, R_{SEI} values of the coated samples prepared by dry coating are larger than those prepared by wet coating. The time constants (τ) corresponding to the charge-transfer reaction, which is indicative of the rate of charge-transfer reaction time in the electrode, is low in all the coated samples except in the wet-coated sample.

At a higher voltage, the Co^{4+} ions in $LiCoO_2$ attack and oxidize the carbonate groups of the solvent molecules due to their acidic/nucleophilic properties and are reduced to Co^{3+} or Co^{2+}.[23] Simultaneously, Co^{4+} ions are capable of oxidizing alkyl carbonates to produce CO_2,[23] resulting in the formation of various organic species at the interfaces.[24] Accordingly, these surface films may be the main sources for increasing the impedances of the uncoated cathode.

However, in coated cathodes prepared by dry coating, such side reactions initiating from Co^{4+} reduction are unlikely. The impedances of the TiO_2-coated electrode prepared from dry coating are

Table III. Resistance and time values of uncoated and coated cathodes before and after cycling at a rate of 1C for 30 cycles under 60°C. Coating concentration was 1 wt %.

	Before cycling				After cycling			
	R_o	R_{SEI}	R_{ct}	τ_{ct} (±0.04 s)	R_o	R_{SEI}	R_{ct}	τ_{ct} (±0.04 s)
Uncoated	5	280	10	0.07	5	25	35	1.3
MgF_2	5	350	9	0.06	5	25	243	8.2
Al_2O_3	5	161	4	0.03	5	25	246	9.2
TiO_2 (dry)	8	150	8	0.05	52	35	85	6.5
TiO_2 (wet)	5	129	5	0.08	5	4	5	0.08

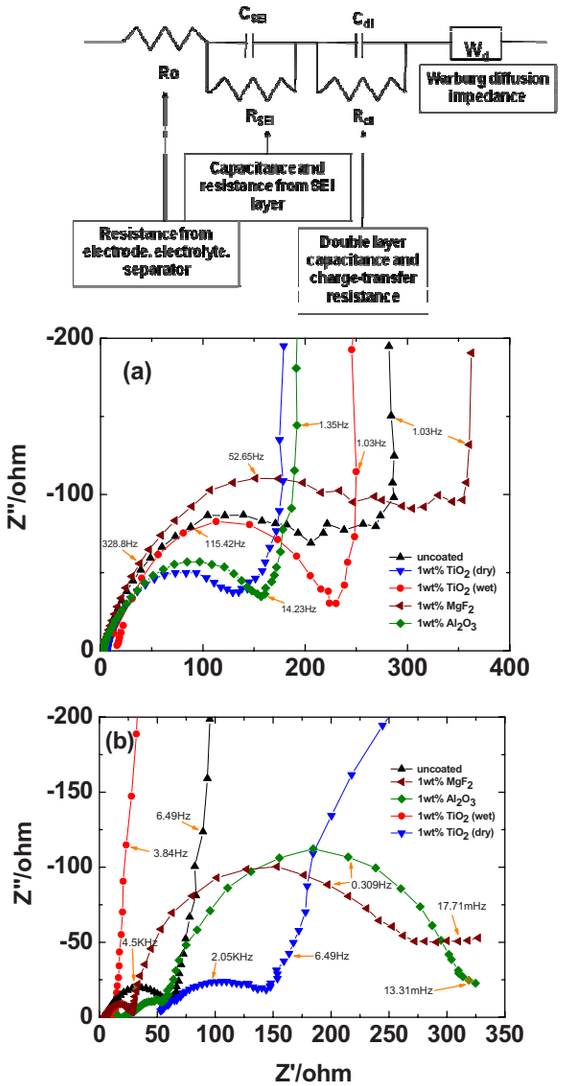

Figure 13. (Color online) Equivalent circuit and Nyquist plots of the uncoated and coated $LiCoO_2$ cathodes with 1 wt % MgF_2, Al_2O_3, and TiO_2 via dry- or wet-coating method (a) before and (b) after 30 cycles at 60°C.

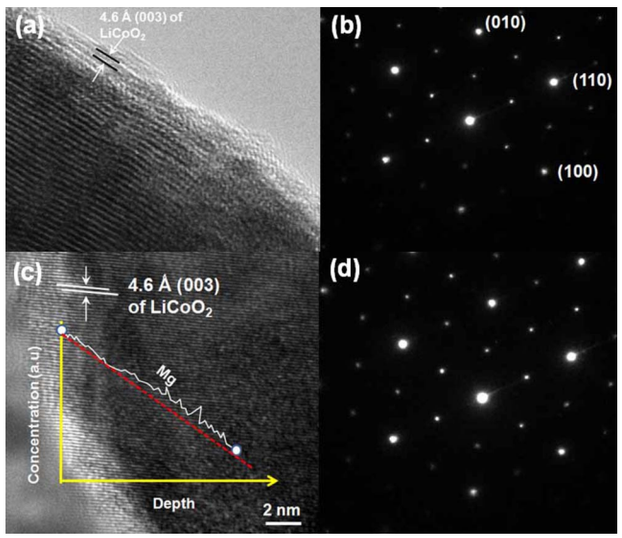

Figure 15. (Color online) HREM images of (a) $AlPO_4$-coated $LiCoO_2$ cathode prepared by dry-coating method, (b) SADP of [(a) and (c)] $MgCO_3$-coated $LiCoO_2$ cathode prepared by dry-coating method, and (d) SADP of (a). Inset of (c) is the distribution of Mg element concentration from the surface to inner particle. Mg concentration (atom %) was measured using an EDX scan along the red line.

much higher than those prepared from wet coating. This result indicates that the unreacted nanoscale coating layer with the $LiCoO_2$ surface that acts as a catalytic site may lead to severe electrolyte decomposition. For instance, LiF and compounds consisting of Li, P, F, and O (e.g., $Li_xPF_yO_z$) may lead to resist Li-ion transport, increasing Li-ion transport through the surface film.[25-28]

To improve such a rapid capacity fade, other coating materials such as $MgCO_3$ and $AlPO_4$ nanoparticles were investigated. Figure 14 shows the XRD patterns of the $MgCO_3$ (0.5 wt %) and $AlPO_4$ (0.2 and 0.5 wt %) coated cathodes prepared by the dry-coating method. All the peaks are assigned to the same phase as the other coated cathodes in Fig. 4. Figure 15 shows the TEM images of these cathodes, and $AlPO_4$ (0.5 wt %) and $MgCO_3$ (0.2 wt %) coated cathodes did not show any coating layer, indicating that $MgCO_3$ and $AlPO_4$ particles were fully incorporated with $LiCoO_2$, thus forming a solid solution. Selected area diffraction patterns (SADPs) (Fig. 15c

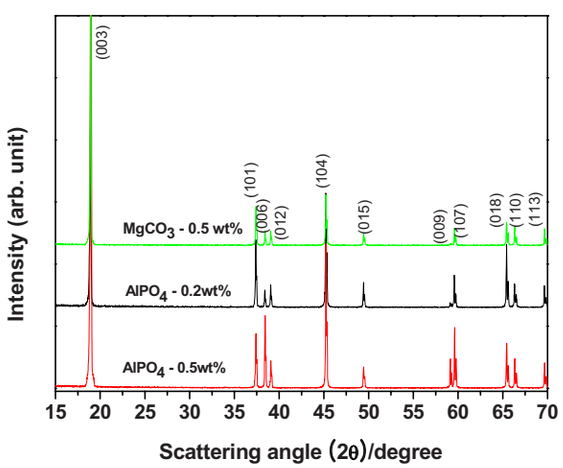

Figure 14. (Color online) XRD patterns of 0.5 wt % $MgCO_3$- and $AlPO_4$-coated $LiCoO_2$ with coating concentrations of 0.2 and 0.5 wt %, respectively.

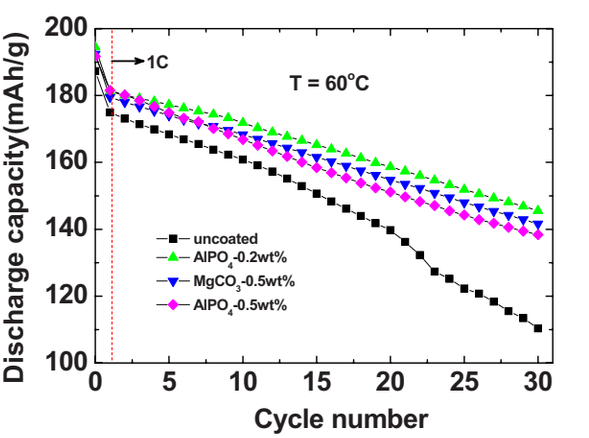

Figure 16. (Color online) Plots of discharge capacity of uncoated and $AlPO_4$ (0.2 and 0.5 wt %) and $MgCO_3$ (0.5 wt %)-coated cathodes under various C rates at 60°C. (After each cycle at a rate of 0.1C, cells were cycled at a rate of 1C for 30 cycles.)

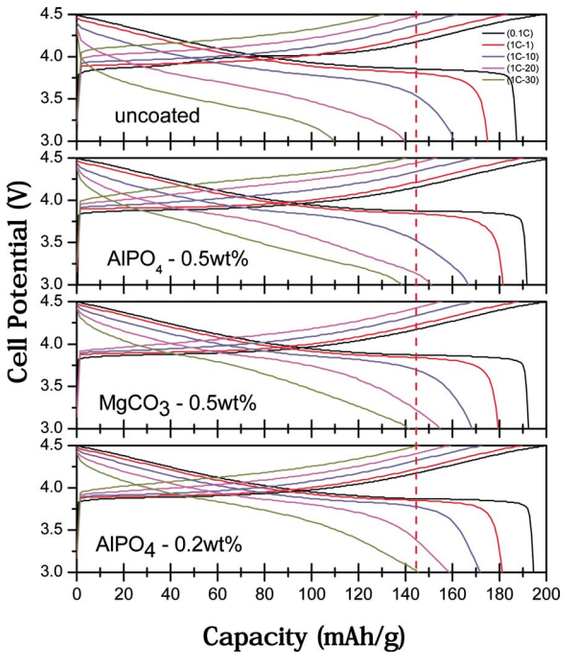

Figure 17. (Color online) Voltage profiles of uncoated and $AlPO_4$- and $MgCO_3$-coated $LiCoO_2$ cathodes at different C rates in coin-type half-cells at 60°C. After 0.1C rate cycle, the cells were cycled at a rate of 1C for 30 cycles.

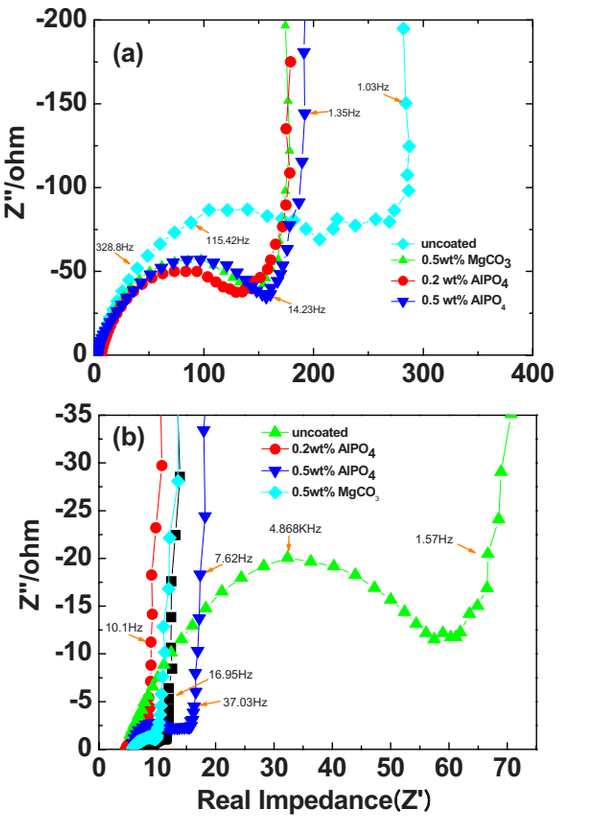

Figure 18. (Color online) Nyquist plots of the uncoated and coated $LiCoO_2$ cathodes with 0.2 and 0.5 wt % $AlPO_4$ and 0.5 wt % $MgCO_3$ via dry-coating method (a) before and after cycling at 60°C. Impedances of the cells were measured before and (b) after 30 cycles (after being fully discharged to 3 V) at a rate of 1C under 60°C.

and d) of the coated samples exhibit only a hexagonal layered phase, supporting the formation of the solid solution. However, lattice constants *a* and *c* remained constant compared with those of the uncoated sample, indicating that the solid solution region was mostly confined near the surface. The distribution of Mg element around the surface area in the coated cathode after $MgCO_3$ coating exhibits the decreasing intensity of Mg elements inward the particle (Fig. 15c).

Figure 16 shows the discharge capacity vs cycle number in the uncoated and coated $LiCoO_2$ with $MgCO_3$ and $AlPO_4$ nanoparticles at 60°C upon cycling at 1C rate. Among them, the 0.2 wt % $AlPO_4$-coated cathode shows the highest discharge capacity and capacity retention even after 30 cycles at 60°C (see Fig. 17). These coated materials exhibit a much improved capacity retention compared to TiO_2-, MgF_2-, and Al_2O_3-coated cathodes. For instance, the capacity retention of 0.5 wt % $MgCO_3$ and 0.2 wt % $AlPO_4$-coated samples is 79 and 88%, respectively. In addition, even in 1C rate cycling, polarization is significantly decreased compared to Al_2O_3-, MgF_2-, and TiO_2-coated samples. This result is well supported by Fig. 18 and Table IV, which show impedance values before and after cycling at 60°C. The values of R_{SEI}, R_{ct}, and T_{ct} in the $MgCO_3$ and $AlPO_4$-coated cathodes are smaller than those of the uncoated and Al_2O_3-, MgF_2-, and TiO_2-coated ones. Accordingly, the selection of coating candidates which enable a complete reaction with $LiCoO_2$ is important to minimize the side reactions with the electrolytes at 60°C.

Conclusion

The dry-coating method was very comparable to the wet-coating method. Compared with Al_2O_3, TiO_2, and MgF_2 coatings, $MgCO_3$ or $AlPO_4$ coating demonstrated a much improved capacity retention at 60°C cycling (>79%). This significant improvement was related to the much reduced side reactions with the electrolytes, which increased the larger formation of nonconducting surface films by the formation of a high metal ion concentration at the surfaces. It is believed that this dry-coating method can be used in other cathodes, such as $LiNi_{1-x}M_xO_2$, olivine, and spinel materials.

Table IV. Resistance and time values of uncoated and coated cathodes before and after cycling at 60°C at a rate of 1C for 30 cycles. Coating concentrations of $MgCO_3$ and $AlPO_4$ were 0.5 and 0.2, 0.5 wt %, respectively.

	Before cycling				After cycling			
	R_o	R_{SEI}	R_{ct}	τ_{ct} (±0.04 s)	R_o	R_{SEI}	R_{ct}	τ_{ct} (±0.04 s)
$MgCO_3$	5	158	2	0.03	5	3	2	0.05
$AlPO_4$	5	144	2	0.04	5	3	2	0.06
$AlPO_4$	5	160	7	0.05	5	6	7	0.07

Acknowledgments

This research was supported by the Converging Research Center Program through the National Research Foundation of Korea (NRF) funded by the Ministry of Education, Science and Technology (2009-0082083). Also, financial support from World Class University (WCU) program is greatly acknowledged.

Ulsan National Institute of Science & Technology assisted in meeting the publication costs of this article.

References

1. M. G. Kim and J. Cho, *Adv. Funct. Mater.*, **19**, 1497 (2009).
2. N. Meethong, Y.-H. Kao, S. A. Speakman, and Y.-M. Chiang, *Adv. Funct. Mater.*, **19**, 1060 (2009).
3. H. Lee, M. G. Kim, and J. Cho, *Electrochem. Commun.*, **9**, 149 (2007).
4. Y. Kim and J. Cho, *J. Electrochem. Soc.*, **154**, A495 (2007).
5. J. Eom and J. Cho, *J. Electrochem. Soc.*, **155**, A201 (2008).
6. Q. Cao, H. P. Zhang, G. J. Wang, Q. Xia, Y. P. Wu, and H. Q. Wu, *Electrochem. Commun.*, **9**, 1228 (2007).
7. J. Cho, *J. Power Sources*, **126**, 186 (2004).
8. J. Cho, Y.-W. Kim, B. Kim, J.-G. Lee, and B. Park, *Angew. Chem., Int. Ed.*, **42**, 1618 (2003).
9. J. Cho, *Electrochem. Commun.*, **5**, 146 (2003).
10. C. Li, H. P. Zhang, L. J. Fua, H. Liu, Y. P. Wu, E. Rahm, R. Holze, and H. Q. Wu, *Electrochim. Acta*, **51**, 3872 (2006).
11. Y. Jin, N. Li, C. H. Chen, and S. Q. Wei, *Electrochem. Solid-State Lett.*, **9**, A273 (2006).
12. G. V. S. Rao, B. V. R. Chowdari, and H. J. Linder, *J. Power Sources*, **97–98**, 313 (2001).
13. H. Kwon, G. Kim, and D. Park, U.S. Pat. 6,183,911 (2001).
14. Y.-K. Sun, S.-W. Cho, S.-W. Lee, C. S. Yoon, and K. Amine, *J. Electrochem. Soc.*, **154**, A168 (2007).
15. M. G. Kim and J. Cho, *J. Mater. Chem.*, **18**, 5880 (2008).
16. G. Li, Z. Yang, and W. Yang, *J. Power Sources*, **183**, 741 (2008).
17. Z. Yang, W. Yang, D. G. Evans, G. Li, and Y. Zhao, *Electrochem. Commun.*, **10**, 1136 (2008).
18. J. Kim, M. Noh, J. Cho, H. Kim, and K.-B. Kim, *J. Electrochem. Soc.*, **152**, A1142 (2005).
19. H. Lee, Y. Kim, Y.-S. Hong, Y. Kim, M. G. Kim, N.-S. Shin, and J. Cho, *J. Electrochem. Soc.*, **153**, A781 (2006).
20. N. Pereira, C. Matthias, K. Bell, F. Badway, I. Plitz, J. Al-Sharab, F. Cosandey, P. Shah, N. Isaacs, and G. G. Amatucci, *J. Electrochem. Soc.*, **152**, A114 (2005).
21. *Advances in Lithium-Ion Batteries*, W. A. Schalkwijk and B. Scrosati, Editors, Kluwer Academic, New York (2002).
22. Y. Wu, A. V. Murugan, and A. Manthiram, *J. Electrochem. Soc.*, **155**, A635 (2008).
23. Z. Wang, Z. Haung, and L. Chen, *J. Electrochem. Soc.*, **151**, A1641 (2004).
24. N. Liu, H. Li, Z. Wang, X. Huang, and L. Chen, *Electrochem. Solid-State Lett.*, **9**, A328 (2006).
25. B. Markovsky, A. Rodkin, G. Salitra, Y. Talyosef, D. Aurbach, and H.-J. Kim, *J. Electrochem. Soc.*, **151**, A1068 (2004).
26. S. K. Martha, H. Sclar, Z. S. Framowitz, D. Kovachva, N. Saliyski, Y. Gofer, P. Sharon, E. Golik, B. Markovsky, and D. Aurbach, *J. Power Sources*, **189**, 248 (2009).
27. Y.-K. Sun, S.-T. Myung, C. S. Yoon, and D.-W. Kim, *Electrochem. Solid-State Lett.*, **12**, A163 (2009).
28. D. Aurbach, *J. Power Sources*, **119–121**, 497 (2003).